

A Role for DEAD Box 1 at DNA Double-Strand Breaks^{∇†}

Lei Li, Elizabeth A. Monckton, and Roseline Godbout*

Department of Oncology, University of Alberta and Cross Cancer Institute, 11560 University Avenue, Edmonton, Alberta T6G 1Z2, Canada

Received 4 July 2008/Returned for modification 28 July 2008/Accepted 7 August 2008

DEAD box proteins are a family of putative RNA helicases associated with all aspects of cellular metabolism involving the modification of RNA secondary structure. DDX1 is a member of the DEAD box protein family that is overexpressed in a subset of retinoblastoma and neuroblastoma cell lines and tumors. DDX1 is found primarily in the nucleus, where it forms two to four large aggregates called DDX1 bodies. Here, we report a rapid redistribution of DDX1 in cells exposed to ionizing radiation, resulting in the formation of numerous foci that colocalize with γ -H2AX and phosphorylated ATM foci at sites of DNA double-strand breaks (DSBs). The formation of DDX1 ionizing-radiation-induced foci (IRIF) is dependent on ATM, which was shown to phosphorylate DDX1 both in vitro and in vivo. The treatment of cells with RNase H prevented the formation of DDX1 IRIF, suggesting that DDX1 is recruited to sites of DNA damage containing RNA-DNA structures. We have shown that DDX1 has RNase activity toward single-stranded RNA, as well as ADP-dependent RNA-DNA- and RNA-RNA-unwinding activities. We propose that DDX1 plays an RNA clearance role at DSB sites, thereby facilitating the template-guided repair of transcriptionally active regions of the genome.

DEAD box proteins, classically defined as putative RNA helicases, have been implicated in all aspects of RNA metabolism involving the modulation of RNA secondary structure (38, 47). These proteins share nine conserved motifs (including the D-E-A-D motif) required for RNA binding, RNA-dependent ATP binding/hydrolysis, and ATP-dependent RNA unwinding. Although >35 DEAD box proteins in higher eukaryotes have been identified, we still have a poor understanding of their biological roles (1). The best-characterized mammalian DEAD box protein is the translation initiation factor eukaryotic initiation factor 4A (eIF4A), which unwinds RNA-RNA and RNA-DNA duplexes in vitro. eIF4A is believed to facilitate translation initiation by removing secondary structures from the 5' ends of transcripts (24).

Analyses of DEAD box proteins in lower eukaryotes and prokaryotes suggest roles in RNA processing, RNA stability, RNA transport, and RNA remodeling. DEAD box proteins (and related DEAH box proteins) have recently been implicated in the DNA damage response, with *Saccharomyces cerevisiae* DHH1 playing a role in G₁/S DNA damage checkpoint recovery (10) and yeast MPH1 proposed to function in a branch of homologous recombination (HR) involved in error-free bypassing of DNA lesions (52). With an estimated >20,000 DNA lesions per cell each day, the effective repair of genomic DNA is critical to the survival of the cell. Of all DNA lesions, double-strand breaks (DSBs) are the most serious threat to the genome, as they can lead to the loss of genetic information, chromosome abnormalities, and cell death. DNA DSBs can be caused by exogenous agents, such as ionizing

radiation (IR), or endogenous agents, such as reactive oxygen species (30). DNA DSBs trigger a sequence of events which include DNA damage sensing, the amplification of damage signals, and the recruitment of the repair machinery, followed by DNA repair and the restoration of normal chromatin structure.

A key player in the DNA DSB response is ATM (*ataxia telangiectasia mutated*), a member of the phosphatidylinositol 3-kinase protein kinase family. Cells from ATM-defective ataxia telangiectasia (A-T) patients show increased chromosome instability and are profoundly defective in their response to DSBs (34). In undamaged cells, ATM exists as a catalytically inactive dimer or higher-order multimer; upon DNA DSB formation, ATM undergoes autophosphorylation, resulting in the formation of catalytically active monomers (3, 32). The *Mre11-Rad50-Nbs1* (MRN) complex is required for the recruitment of activated ATM to DNA DSB sites (21, 35), where ATM in turn amplifies and sustains the DNA damage signaling cascade through the recruitment and phosphorylation of additional proteins involved in signal transduction and DNA repair (54). Substrates of activated ATM include p53, H2AX, Nbs1, BRCA1, 53BP1, and ATM itself.

The DEAD box 1 gene (*DDX1*) is a widely expressed gene that is amplified in a subset of retinoblastoma and neuroblastoma cell lines and tumors (25, 26). In addition to the nine motifs characteristic of DEAD box proteins, the DDX1 protein contains a 130-amino-acid SPRY domain in its N-terminal region (25, 43). DDX1 is found primarily in the nucleus, where it has a punctate distribution pattern. DDX1 also forms distinct foci, called DDX1 bodies, in the nucleus (11). A close spatial relationship among DDX1 bodies, cleavage bodies, and Cajal bodies (CBs) has been observed previously, with DDX1 bodies and cleavage bodies colocalizing and residing adjacent to CBs (37). Cleavage bodies and CBs are enriched with proteins associated with RNA metabolism and have been proposed to serve as storage/assembly sites for proteins involved in

* Corresponding author. Mailing address: Department of Oncology, Cross Cancer Institute, 11560 University Avenue, Edmonton, Alberta T6G 1Z2, Canada. Phone: (780) 432-8901. Fax: (780) 432-8892. E-mail: roseline@cancerboard.ab.ca.

† Supplemental material for this article may be found at <http://mcb.asm.org/>.

∇ Published ahead of print on 18 August 2008.

transcription, splicing, 3'-end processing of pre-mRNAs, and RNA degradation (22).

Upon the treatment of cells with IR, we observed a rapid redistribution of DDX1 protein into multiple foci (IR-induced foci [IRIF]) within the nucleus. A coimmunofluorescence analysis revealed the extensive colocalization of DDX1 foci with activated γ -H2AX and phosphorylated ATM (pATM) at sites of DNA DSBs. However, whereas virtually every DDX1 IRIF colocalized with γ -H2AX and pATM IRIF, only a subset of γ -H2AX and pATM IRIF colocalized with DDX1, suggesting a specialized role for DDX1-containing IRIF. The inactivation of ATM resulted in a loss of IR-induced DDX1 foci, directly linking DDX1 to the ATM signaling pathway. The data presented in this paper support a role for DDX1 in the repair of transcriptionally active regions of the genome.

MATERIALS AND METHODS

Cell culture and drug treatment. The following human cell lines were used: HeLa, cervical carcinoma cells; GM38, normal lung fibroblasts; RB522A, retinoblastoma cells with amplified *DDX1*; RB805, retinoblastoma cells with no amplification of *DDX1*; U2OS and Saos2, osteosarcoma cells; U251, malignant glioma cells; M059J, DNA-PKcs-negative malignant glioma cells; M059K, DNA-PKcs-positive malignant glioma cells; AT2BE and AT5BI, ATM-deficient primary fibroblasts established from A-T patients; pEBS7 (EBS) and pEBS7-YZ5 (YZ5), simian virus 40-transformed cells from the same A-T patient, with YZ5 cells expressing full-length ATM and EBS cells transfected with a control vector; and BT and L3, ATM-positive normal lymphoblastoid cells and ATM-negative A-T patient lymphoblastoid cells, respectively.

Cells were irradiated using a ^{137}Cs irradiator (Shepherd, San Fernando, CA). Recovery was at 37°C for the lengths of time indicated below. Cells were treated with the following chemicals: 20 μM wortmannin (Sigma) for 1 h prior to radiation, 6 $\mu\text{g}/\text{ml}$ actinomycin D (Sigma) for 30 min prior to irradiation, and 80 $\mu\text{g}/\text{ml}$ bleomycin (Mayne Pharma Pty. Ltd., Australia) for 2 h prior to fixation. To enrich for cells in mitosis, HeLa cells were blocked in 2.5 mM thymidine for 12 h. Cells were released from the thymidine block and exposed to 5 Gy of γ -irradiation 10 h later, at which time ~60% of cells were in mitosis.

Fluorescence microscopy. Cells adhering to coverslips were fixed and processed as described previously (37). Cells were immunostained with the following antibodies: rabbit anti-DDX1 (batch 2923; 1:1,000 dilution) (11), mouse monoclonal anti- γ -H2AX (1:4,000; Upstate Biotechnology), a mouse monoclonal antibody to ATM phosphorylated at Ser1981 (anti-pATM^{Ser1981} [1:2,000; Rockland]), mouse anti-promyelocytic leukemia protein (anti-PML [1:1,000; a gift from Roel van Driel, University of Amsterdam]), mouse anti-Sm Y12 (1:3,000; a gift from Joan Steitz, Yale University), mouse anti-CstF64 (1:1,000; a gift from James Manley, Columbia University), and anti-RNA polymerase II (H5; 1:200) (12). For antibody competition experiments, the anti-DDX1-anti- γ -H2AX antibody mixture was incubated with 1.5 $\mu\text{g}/\text{ml}$ recombinant DDX1 before immunostaining.

To examine the colocalization of DDX1 foci, γ -H2AX foci, and/or pATM foci on a three-dimensional scale, stacks of 20 to 30 images (*z*-series) taken at 0.3- μm intervals were collected. Cell images were three-dimensionally reconstructed using the Imaris program (version 4.1.1; Bitplane AG Corp., Zurich, Switzerland). Images were corrected for background staining by subtracting background values. In order to remove shot noise from the detector, a 3X3X1 median filter was applied to each image. Each image was then surface rendered (in the surpass mode in Imaris) using intensity threshold values specific to each antibody. These values were determined by comparing the numbers of foci defined at specific threshold values with the numbers of clear-cut foci observed under the microscope. These threshold values were used as guides throughout the analysis. A minimum of 30 cell images were three-dimensionally reconstructed and analyzed for each parameter tested (at each time point or dose).

Coimmunoprecipitation and Western blot analysis. Whole-cell extracts were prepared by resuspending the cells in lysis buffer (50 mM Tris-HCl, pH 7.5, 150 mM NaCl, 0.5% sodium deoxycholate, 1% NP-40, 50 mM NaF, 1 mM Na_3VO_4 , 25 mM sodium pyrophosphate, and Complete protease inhibitors [Roche]). Coimmunoprecipitation was carried out with lysis buffer containing 0.1% sodium deoxycholate and 0.2% NP-40. Approximately 1 mg of whole-cell extract was incubated with 5 μl of rabbit anti-DDX1 antibody (batch 2910) (11) or 6 μl of rabbit anti-ATM antibody. Immunoprecipitates were washed three times, elec-

TABLE 1. RNA and DNA oligonucleotides used in this study^a

Designation	Sequence (5'→3')
R41(+)GAAUACAAGCUUGCAUGCCUGCAGGUCGACUCUAGAGGAUC
R29(-)GAUCCUCUAGAGUCGACCCUGCAGGCAUGC
D41(+)GAATACAAGCTTGCATGCCTGCAGGTTCGACTCTAGAGGATC
D29(-)GATCCTCTAGAGTCGACCTGCAGGCATGC
D41(-)GATCCTCTAGAGTCGACCTGCAGGCATGCAAGCTTGTATTTC
D29(+)GCATGCCTGCAGGTTCGACTCTAGAGGATC

^a The complementary sequences of the 41-mer and the 29-mer are underlined. + and - indicate opposite strand polarities. Note that the sequences of D41(+) and D29(-) are the exact DNA counterparts of the sequences of R41(+) and R29(-), respectively. R41(+) and R29(-) are complementary to D41(-) and D29(+), respectively.

trophoresed in a low-bis sodium dodecyl sulfate (SDS)-8% polyacrylamide gel, and then transferred onto nitrocellulose. Blots were immunostained with mouse anti-ATM antibody (1:200; Santa Cruz), mouse anti-Mre11 antibody (1:1,000; BD Transduction Laboratories), rabbit anti-Nbs1 antibody (1:5,000; Novus Biologicals), sheep anti-Rad50 antibody (1:2,000; Abcam), goat anti-ATR antibody (1:200; Santa Cruz), and rabbit anti-DDX1 antibody (1:5,000).

ATM kinase assay. The *in vitro* ATM kinase assay was performed using a modification of the protocol described by Canman et al. (15). Briefly, pelleted cells were washed with phosphate-buffered saline (PBS) and lysed in a mixture of 50 mM Tris-HCl, pH 7.5, 150 mM NaCl, 10% glycerol, 1% Tween 20, 200 mM microcystin-LR, 10 mM NaF, 1 mM Na_3VO_4 , and 1 \times Complete protease inhibitor cocktail by being syringed through a 25-gauge needle. Endogenous ATM was immunoprecipitated from ~500 μg of whole-cell lysate by using anti-ATM mouse monoclonal antibody SYR6D4 (Sigma). Immunoprecipitates were washed twice in lysis buffer, three times in 100 mM Tris-HCl (pH 7.5)-1.0 M LiCl, twice in prekinase buffer (20 mM HEPES, pH 7.5, 50 mM NaCl, 10 mM MgCl_2 , 1 mM dithiothreitol, 200 mM microcystin-LR, and 1 mM NaF), and once in kinase buffer (prekinase buffer supplemented with 10 mM MnCl_2). Immunoprecipitates were resuspended in 30 μl of kinase buffer and incubated with a mixture of 2 μg of recombinant DDX1 and 10 μCi of [γ - ^{32}P]ATP (3,000 Ci/mmol; GE Healthcare) at 30°C for 20 min. Where indicated, 2 μM wortmannin was included in the kinase reaction. Proteins were electrophoresed in SDS-polyacrylamide gel electrophoresis (PAGE) gels and transferred onto nitrocellulose membranes by electroblotting. Phosphorylated DDX1 was visualized by autoradiography.

Metabolic labeling with $^{32}\text{P}_i$. HeLa cells at ~80% confluence were labeled with $^{32}\text{P}_i$ (PBS13; GE Healthcare) in phosphate-free Dulbecco's modified Eagle's medium for 10 min before treatment with 5 Gy of IR. One hour later, cells were lysed in lysis buffer at 4°C. Where indicated, cells were pretreated with 100 μM wortmannin for 30 min before exposure to IR. One milligram of precleared ^{32}P -labeled whole-cell extract was incubated with 5 μl of anti-DDX1 antibody overnight at 4°C. Immunoprecipitates were washed in lysis buffer and subjected to PAGE. The ^{32}P -labeled proteins were visualized by autoradiography. To visualize DDX1, the same blots were immunostained with anti-DDX1 antibody.

DNase and RNase treatment. Cells were exposed to 5 Gy of IR and incubated at 37°C for 1 h. The cells were then permeabilized (in a solution of 2% Tween 20 in PBS for 10 min at room temperature) and treated with DNase I (20 U; Roche), RNase A (0.1 mg; USB Corporation), or RNase H (5 U; USB Corporation) in 100 μl of PBS containing 5 mM MgCl_2 per coverslip for 15 min at room temperature. Cells were fixed and immunostained as described above.

Unwinding assays. Two RNA oligonucleotides and four DNA oligonucleotides were used to generate the various RNA-DNA, and RNA-DNA, and DNA-DNA heteroduplexes used for the unwinding assays. R41(+) (top strand) RNA was prepared by the transcription of a BamHI-digested pGEM3 plasmid with SP6 RNA polymerase, followed by PAGE purification as described previously (41). R29(-) (bottom strand) RNA was synthesized and PAGE purified by Pharmacia. D29(+), D29(-), D41(+), and D41(-) DNA oligonucleotides were synthesized by Invitrogen. The sequences of RNA and DNA oligonucleotides are given in Table 1.

RNA and DNA oligonucleotides were 5' end labeled with [γ - ^{32}P]ATP (3,000 Ci/mmol; GE Healthcare) by using T4 polynucleotide kinase (New England Biolabs). ^{32}P -labeled oligonucleotides were annealed with equimolar amounts of unlabeled complementary strands in annealing buffer (20 mM Tris-HCl, pH 7.5, 200 mM potassium acetate, 0.1 mM EDTA). The mixture was heated at 95°C for 2 min, slowly cooled to room temperature, and then incubated at room temper-

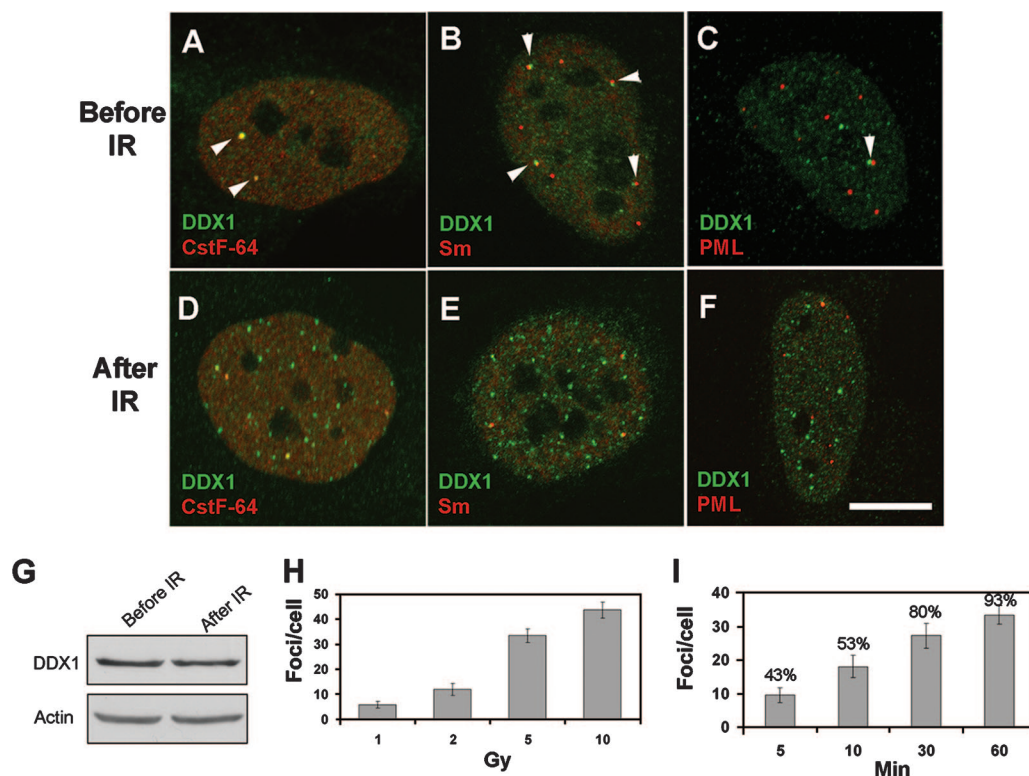


FIG. 1. Formation of DDX1 IRIF upon exposure to γ -rays. (A to F) HeLa cells were grown on glass coverslips and exposed to 5 Gy of IR. One hour later, control cells (A to C) and irradiated cells (D to F) were fixed and double stained with anti-DDX1 antibody and anti-CstF64 (A and D), anti-Sm (B and E), and anti-PML (C and F) antibodies. Arrowheads indicate associations between DDX1 bodies and cleavage bodies (A), DDX1 bodies and CBs (B), and DDX1 bodies and PML bodies (C). Bar, 10 μ m. (G) Whole-cell extracts from control HeLa cells and HeLa cells exposed to 5 Gy of IR were prepared. Fifty micrograms of protein was loaded into each lane. (H) Dose dependence of DDX1 IRIF. HeLa cells were exposed to 1, 2, 5, and 10 Gy and examined after 1 h of recovery. The number of foci per cell as a function of the radiation dose is indicated. (I) Time course of DDX1 IRIF formation. HeLa cells were exposed to 5 Gy of IR and examined at the time points indicated. The percentage of cells containing DDX1 IRIF at each time point is shown. Bars refer to standard errors of the means.

ature for 2 h to allow duplex formation. This method resulted in the incorporation of $\geq 80\%$ of the labeled strand into the annealed duplex.

A construct comprising the glutathione *S*-transferase gene fused to the entire coding region of the DDX1 gene was bacterially expressed, and the fusion protein was purified with glutathione-Sepharose 4B. Glutathione *S*-transferase was cleaved with thrombin. Unwinding assays were carried out in a 20- μ l reaction volume using 50 fmol of radiolabeled DNA and/or RNA substrates and 0.3 μ g (3.6 pmol) of recombinant DDX1 protein in a mixture of 20 mM Tris-HCl, pH 7.5, 70 mM KCl, 2 mM magnesium acetate, 1.5 mM dithiothreitol, and 10 U of RNAGuard (GE Healthcare). Where indicated, ATP, ATP- γ -S, ADP, or GTP was added to a final concentration of 1 mM. For reactions without Mg^{2+} , 10 mM EDTA, pH 7.5, was also included. Reaction mixtures were incubated at 37°C for 20 min, and reactions were quenched with ice. Five microliters of loading buffer (50 mM EDTA, 40% glycerol) was added to each sample, and the samples were electrophoresed through a 12% native polyacrylamide gel (acrylamide/bisacrylamide, 29:1) in 1 \times Tris-borate-EDTA buffer. Gels were dried and exposed to X-ray film.

RESULTS

Formation of DDX1 irradiation-induced foci upon exposure to IR. We previously demonstrated an association between DDX1 bodies, cleavage bodies, and CBs during the S phase of the cell cycle, with DDX1 bodies and cleavage bodies colocalizing and residing adjacent to CBs (37). We further demonstrated that the inhibition of DNA replication by using aphidicolin and hydroxyurea leads to the disassembly of CstF64-containing cleavage bodies. As DNA damage

also inhibits DNA synthesis (7), we pursued these observations by studying the effect of IR on nuclear bodies. HeLa cells were exposed to 5 Gy of IR and allowed to recover for 1 h. Nuclear bodies were then analyzed by immunofluorescence. Whereas the numbers of cleavage bodies (detected with anti-CstF64 antibody) and CBs (detected with anti-Sm antibody) remained largely unchanged after exposure to IR, the number of DDX1 bodies increased from an average of 2 to 4 per cell pre-IR to 30 to 40 per cell post-IR (Fig. 1A to F). Other agents, such as UV light and cisplatin, did not lead to the immediate formation of DDX1 IRIF (see Fig. S1 in the supplemental material). In contrast, DDX1 IRIF were observed in 90% of cells treated with bleomycin, a radiomimetic drug that causes DSBs (Fig. 2C, left panel). The formation of DDX1 IRIF appeared to be mediated through DDX1 protein relocalization, as no change in pre-IR DDX1 protein levels was observed post-IR (Fig. 1G).

PML nuclear bodies have been shown previously to increase in number upon IR, from a mean of 17 (pre-IR) to a mean of 24 upon exposure to 10 Gy of IR (20). As we had previously observed the occasional adjacent localization of DDX1 bodies and PML bodies in nonirradiated HeLa cells (11) (Fig. 1C), we examined the association of DDX1 and PML bodies after IR. No increase in either the adjacent localization or the colocal-

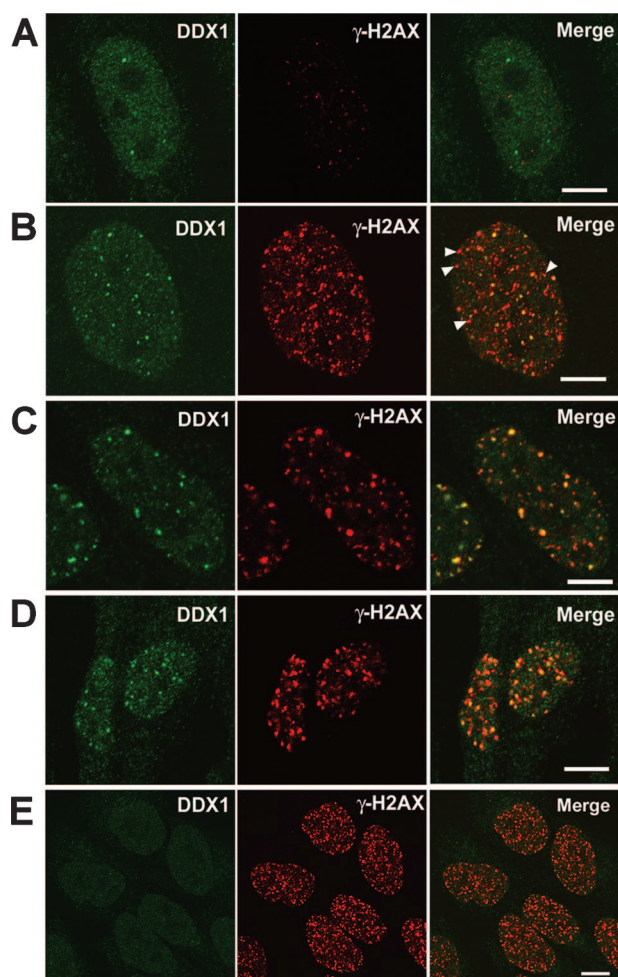


FIG. 2. Colocalization of DDX1 IRIF with γ -H2AX foci. (A and B) Control HeLa cells (A) and HeLa cells treated with 5 Gy of IR (B) were examined 1 h after IR. Arrowheads indicate γ -H2AX foci that have no DDX1. (C) HeLa cells were treated with 80 μ g/ml bleomycin for 2 h and subjected to immunostaining. (D) Normal GM38 fibroblasts were fixed 60 min after exposure to 5 Gy of IR and double stained with anti-DDX1 and anti- γ -H2AX antibodies. (E) An anti-DDX1 and anti- γ -H2AX antibody mixture was incubated with 1.5 μ g/ml of a recombinant DDX1 peptide (amino acids 1 to 186) as a competitor for 4 h at room temperature. Double immunostaining of irradiated HeLa cells was then carried out as described in the legend to panel D. Bars, 10 μ m.

ization of DDX1 IRIF and PML bodies was observed upon the exposure of HeLa cells to 5 Gy of IR (Fig. 1F). These data suggest that DDX1 and PML act in different cellular pathways in response to DNA DSBs.

To determine whether the induction of DDX1 IRIF is dose dependent, HeLa cells were exposed to 1, 2, 5, and 10 Gy of IR and immunostained 1 h later. A direct correlation between the DDX1 IRIF number and the IR dose was observed, with the number of DDX1 foci increasing from an average of 5 at 1 Gy to 40 at 10 Gy (Fig. 1H). Furthermore, DDX1 IRIF could be visualized as early as 5 min after exposure to 5 Gy of IR, with 43% of cells being positive for these foci. More than 90% of cells were positive for DDX1 IRIF after 1 h (Fig. 1I). The

formation of DDX1 IRIF, therefore, represents an early response to IR exposure.

The examination of GM38 (normal human fibroblasts), U2OS and Saos2 (osteosarcoma cells), RB522A and RB805 (retinoblastoma cells with and without the amplification of *DDX1*), and U251 (malignant glioma cells) revealed DDX1 IRIF in all these cell types upon exposure to IR. The presence of DDX1 IRIF in GM38 cells indicates that these foci are not restricted to transformed cells (Fig. 2D, left panel).

Colocalization of DDX1 IRIF and γ -H2AX foci. H2AX is a histone 2A variant containing a Ser139 residue that is rapidly phosphorylated upon the exposure of cells to IR, resulting in the formation of γ -H2AX foci at sites of DNA DSBs (48). There is good correlation between the number of γ -H2AX IRIF and the estimated number of DNA DSBs upon exposure to IR, with 1 Gy producing 20 to 30 DNA DSBs and approximately the same number of γ -H2AX foci (50).

To investigate a possible relationship between DDX1 IRIF and DNA DSBs, we studied the subcellular localization patterns of DDX1 foci and γ -H2AX foci after IR treatment. As shown in Fig. 2A, there was no association between DDX1 bodies and γ -H2AX foci before irradiation. However, the vast majority of DDX1 foci and γ -H2AX foci had colocalized at 1 h post-IR in cells treated with 5 Gy (Fig. 2B, far-right panel). Colocalization was also observed at earlier time points after irradiation (data not shown). To ensure that the signal detected with anti-DDX1 antibody at DNA DSBs was indeed due to DDX1, we carried out competition experiments with a recombinant DDX1 peptide (amino acids 1 to 186, the immunogen used to produce the anti-DDX1 antibody). For these experiments, anti-DDX1 and anti- γ -H2AX antibodies were preincubated with the recombinant DDX1 peptide prior to immunostaining. DDX1 IRIF were completely absent from irradiated cells stained with pretreated antibodies, with no change in the signal intensity observed for γ -H2AX IRIF (Fig. 2E).

Considerably more γ -H2AX foci than DDX1 foci were observed in irradiated cells (Fig. 2B). To further document this discrepancy in numbers of foci, we generated z-stack images of 30 DDX1 and γ -H2AX double-stained cells, which were then three-dimensionally reconstructed using Imaris software. The colocalization analysis of reconstructed cell images revealed that 72% of DDX1 foci colocalized with γ -H2AX foci, in contrast to the 29% of γ -H2AX foci that colocalized with DDX1 foci. These data suggest that DDX1 assembles at only a subset of DNA DSBs.

DDX1 IRIF formation requires functional ATM, but not DNA-PKcs. Three phosphatidylinositol 3-kinase-related proteins, ATM, ATR, and DNA-PKcs, are critical players in DNA damage response pathways. While ATM and DNA-PKcs are involved primarily in DNA DSB repair, ATR participates mainly in cellular responses to UV damage and stalled replication forks (2), although cross talk between ATM and ATR has been reported previously (27). ATM, ATR, and DNA-PKcs have all been shown to phosphorylate H2AX upon DNA damage (56, 60). To investigate whether DDX1 IRIF formation was dependent on any one of these kinases, we treated cells with 20 μ M wortmannin, a concentration that inhibits ATM and DNA-PKcs but not ATR (51), followed by 5 Gy of IR. As shown in Fig. 3A, wortmannin significantly reduced the

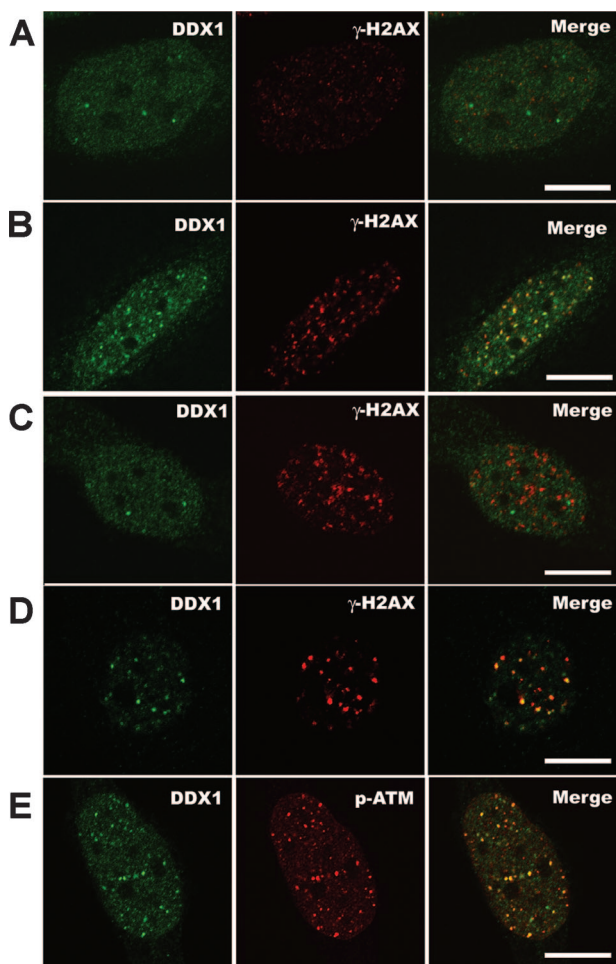


FIG. 3. The formation of DDX1 IRIF requires functional ATM. (A) HeLa cells were pretreated with 20 μ M wortmannin for 1 h and then subjected to 5 Gy of IR. Cells were immunostained after 1 h of recovery. (B, C, and D) DNA-PKcs-deficient M059J cells (B), ATM-deficient EBS cells (C), and ATM-expressing YZ5 cells (D) were treated with 5 Gy of IR. Cells were immunostained as described in the legend to panel A. (E) HeLa cells were treated with IR (5 Gy) and immunostained with anti-DDX1 and anti-pATM^{Ser1981} antibodies 1 h post-IR. Bars, 10 μ m.

number of DDX1 IRIF, suggesting that ATM and/or DNA-PKcs is required for DDX1 IRIF formation.

To address a possible role for DNA-PKcs in DDX1 IRIF formation, we examined the paired cell lines M059K and M059J, proficient and deficient in DNA-PKcs, respectively (36). M059K and M059J cells showed normal numbers of DDX1 nuclear bodies prior to irradiation (data not shown). Exposure to IR resulted in the formation of DDX1 and γ -H2AX IRIF in both cell lines (M059J cells are shown in Fig. 3B). Thus, DNA-PKcs is dispensable for DNA DSB-induced DDX1 focus formation.

Next, we examined DDX1 IRIF formation in three ATM-deficient fibroblast lines: EBS (63), AT2BE (6), and AT5BI (55). While DDX1 nuclear bodies were present in all three cell cultures prior to IR, there was no change in the numbers and appearance of these nuclear bodies after IR (EBS cells are shown in Fig. 3C). In contrast, γ -H2AX foci were induced in all

three cultures after exposure to IR. The expression of functional ATM in cells of the YZ5 line, an isogenic derivative of the EBS line, restored the formation of DDX1 IRIF, albeit at lower numbers than those observed in cells that naturally express ATM (Fig. 3D). These results indicate a role for ATM in the response of DDX1 to IR.

When cells are exposed to IR, pATM accumulates at DNA DSBs (3). The coimmunostaining of irradiated HeLa cells with anti-DDX1 antibody and anti-pATM^{Ser1981} antibody revealed extensive colocalization of DDX1 and pATM IRIF (Fig. 3E). The analysis of three-dimensionally reconstructed z-stack images showed that 91% of DDX1 foci colocalized with pATM foci in irradiated cells, whereas 46% of pATM foci colocalized with DDX1 foci, in support of the conclusion that DDX1 foci accumulate at a subset of DNA DSBs.

Coimmunoprecipitation of DDX1, ATM, and the MRN complex. The colocalization of DDX1 and pATM IRIF suggests that DDX1 and pATM may reside in the same cellular complex. To test this possibility, we carried out reciprocal coimmunoprecipitations of DDX1 and ATM. Using anti-DDX1 antibody, we were able to immunoprecipitate endogenous ATM (Fig. 4A, top panel). Similarly, DDX1 coimmunoprecipitated with endogenous ATM when anti-ATM antibody was used (Fig. 4B). The amounts of coimmunoprecipitated DDX1 and ATM in control and irradiated cells were similar, suggesting that DDX1 and ATM can exist in the same complex in the absence of DNA damage. The proportion of ATM that coimmunoprecipitated with DDX1 (and vice versa) was small (~1%), indicating either a weak interaction between the two proteins or an association limited to a subset of DDX1 and ATM proteins. These results are similar to those reported by others upon the coimmunoprecipitation of ATM with known binding partners of ATM, such as Nbs1 and BRCA1 (18). ATR was not detected in the DDX1 immunocomplex, providing further evidence that ATR is not involved in IR-induced DDX1 relocalization (Fig. 4A).

The MRN complex plays a key role in IR-induced cellular responses. It has been proposed previously that the MRN complex recognizes and processes DNA DSBs and relays this information to ATM (54). All three components of the MRN complex, Mre11, Rad50, and Nbs1, were detected in the anti-DDX1 immunocomplex (Fig. 4A), providing additional evidence that DDX1 accumulates at DNA DSB sites. As observed for ATM, components of the MRN complex associated with DDX1 whether the cells were irradiated or not, although the intensity of the signal in lysates derived from irradiated cells was slightly stronger than that in lysates from control cells (Fig. 4A).

In vitro and in vivo phosphorylation of DDX1. The colocalization and coimmunoprecipitation of DDX1 and ATM raise the possibility that DDX1 is a substrate of the ATM kinase. Sequence analysis of DDX1 reveals five consensus S/TQ motifs that may be phosphorylated by ATM (31). We therefore tested whether ATM was able to phosphorylate DDX1 in vitro. Endogenous ATM was immunoprecipitated from HeLa cells and incubated with recombinant DDX1 in the presence of [γ -³²P]ATP. As shown in Fig. 4C, DDX1 was phosphorylated by ATM in vitro. DDX1 phosphorylation was strictly dependent on Mn²⁺ and significantly inhibited by wortmannin (Fig. 4C), consistent with wortmannin's inhibition of ATM kinase

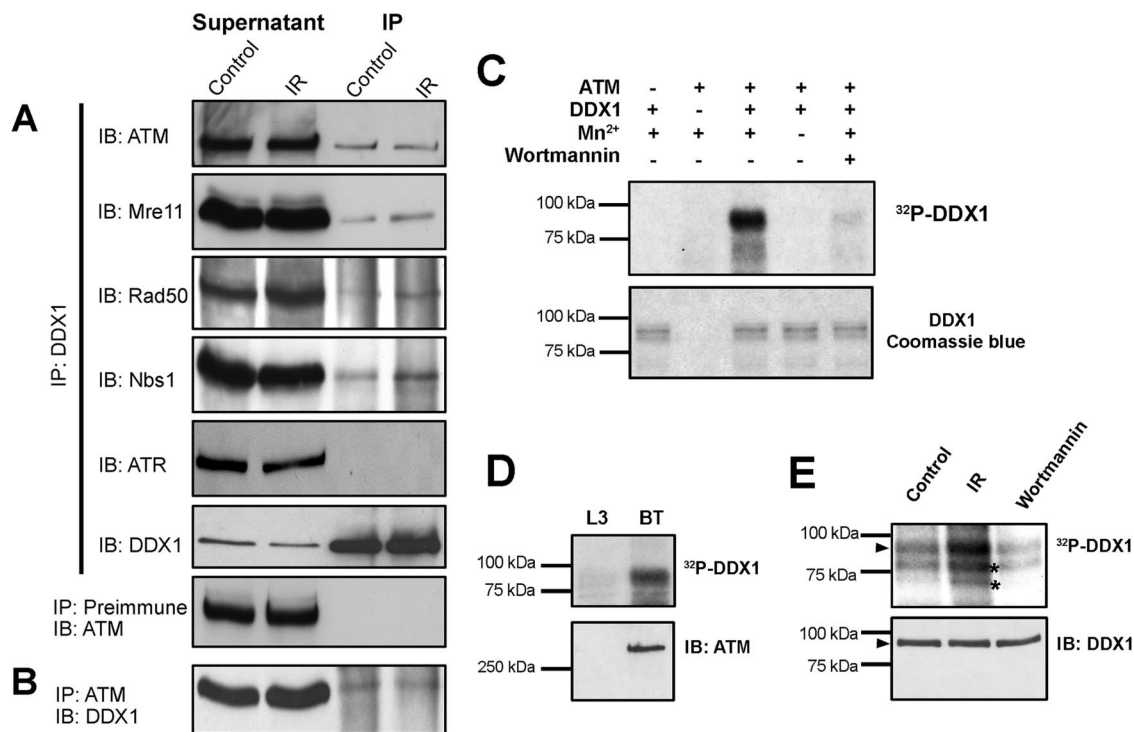


FIG. 4. Coimmunoprecipitation and phosphorylation of DDX1. (A) Whole-cell extracts from control and irradiated (IR) HeLa cells were incubated with either anti-DDX1 antibody or preimmune serum. The immunocomplexes were subjected to electrophoresis, transferred, and probed with the antibodies indicated. Six percent of the supernatant from each immunoprecipitation was loaded into the indicated lanes. IP, immunoprecipitation; IB, immunoblotting. (B) HeLa whole-cell extracts were immunoprecipitated with anti-ATM antibody. DDX1 was detected with anti-DDX1 antibody. (C) Endogenous ATM protein was immunoprecipitated from HeLa whole-cell extracts using anti-ATM antibody. The immunocomplex was incubated with 2 μ g of recombinant DDX1 protein at 30°C for 20 min in the presence of [γ -³²P]ATP. Samples were divided and electrophoresed through two replicate SDS-10% PAGE gels. One gel (top panel) was transferred onto nitrocellulose, and the filter was exposed to film to detect phosphorylated DDX1. The second gel (bottom panel) was stained with Coomassie blue to allow the visualization of the recombinant DDX1 substrate used in each reaction. +, present; -, absent. (D) Endogenous ATM protein was immunoprecipitated from BT (ATM-proficient) and L3 (ATM-deficient) cells. The *in vitro* ATM kinase assay was performed as described in the legend to panel C. The phosphorylation of DDX1 was visualized by autoradiography. Immunoprecipitated ATM was detected with anti-ATM antibody using the same membrane. (E) Control HeLa cells and HeLa cells subjected to IR (5 Gy) were metabolically labeled with ³²P_i. Endogenous DDX1 protein from metabolically labeled cells was immunoprecipitated with anti-DDX1 antibody. The immunocomplex was fractionated in an SDS-PAGE gel and transferred, and phosphorylated DDX1 protein was visualized by autoradiography. The identity of DDX1 was confirmed by immunostaining the membrane with anti-DDX1 antibody. Where indicated, cells were pretreated with 100 μ M wortmannin for 30 min before IR. Asterisks indicate coimmunoprecipitated unknown proteins that were also phosphorylated.

activity and the requirement for Mn²⁺ for ATM kinase activity (5, 15). To further document the role of ATM in DDX1 phosphorylation, we carried out *in vitro* phosphorylation experiments with extracts from BT (ATM-proficient) and L3 (ATM-deficient) cells. As shown in Fig. 4D, recombinant DDX1 was phosphorylated by ATM immunoprecipitates derived from BT cells but not those from L3 cells.

Next, we examined the *in vivo* phosphorylation status of DDX1 as a consequence of exposure to IR. HeLa cells were metabolically labeled with ³²P, subjected to 5 Gy of IR, and lysed 1 h later. Endogenous DDX1 was immunoprecipitated from the cell lysates, electrophoresed through an SDS-PAGE gel, and transferred onto nitrocellulose membranes. Although there was a basal level of phosphorylated DDX1 prior to IR, phosphorylation was significantly increased (>3-fold) in response to IR (Fig. 4E). The treatment of cells with wortmannin prior to irradiation greatly reduced levels of phosphorylated DDX1 (Fig. 4E). These results suggest a link between DDX1 phosphorylation and DDX1 relocalization in response to IR.

DDX1 IRIF and RNA transcription. DEAD box proteins are putative RNA helicases that alter RNA secondary structure. These proteins bind RNA and have RNA-dependent ATPase and ATP-dependent RNA-unwinding activities. The accumulation of a putative RNA-unwinding protein at sites of DNA DSBs suggests a connection between RNA and DNA DSB repair. To address the possibility that DDX1 may be associated with sites of active transcription at DNA DSBs, we carried out coimmunostaining with anti-RNA polymerase II (active-form) antibodies and anti-DDX1 antibodies. There was no accumulation of RNA polymerase II at DDX1 IRIF, with RNA polymerase II showing a speckled staining pattern throughout the nucleus (see Fig. S2A in the supplemental material). Furthermore, neither the phosphorylated (active) nor the unphosphorylated (inactive) form of RNA polymerase II coimmunoprecipitated with DDX1 before or after IR (see Fig. S2B in the supplemental material). Attempts to correlate DDX1 IRIF with newly synthesized RNA by labeling with 5-fluorouridine (5-FUrd) for 15 min prior to irradiation were equally unsuc-

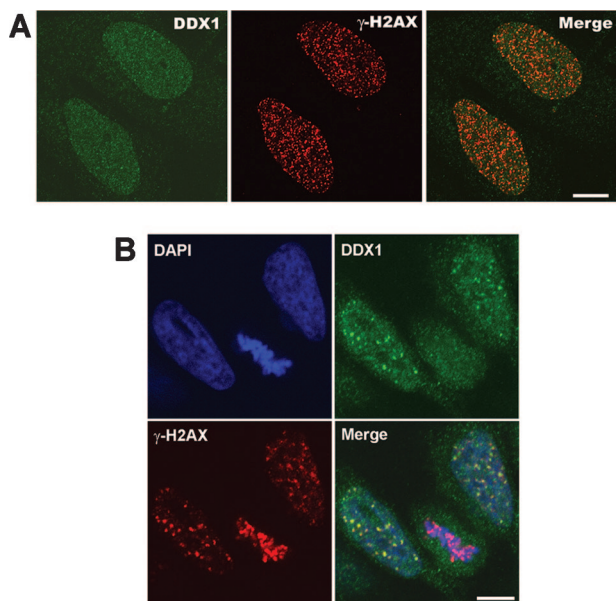


FIG. 5. DDX1 IRIF and transcription. (A) HeLa cells were incubated with 6 $\mu\text{g/ml}$ of actinomycin D for 30 min and exposed to 5 Gy of IR. One hour later, cells were fixed and immunostained with anti-DDX1 and anti- $\gamma\text{-H2AX}$ antibodies. (B) Ten hours after release from the thymidine block, HeLa cells were exposed to 5 Gy of IR and immunostained with anti-DDX1 and anti- $\gamma\text{-H2AX}$ 30 min post-IR. Bars, 10 μm . DAPI, 4',6-diamidino-2-phenylindole.

successful, with anti-BrdU antibody staining showing a speckled pattern throughout the nucleus, with intense staining in the nucleolus (see Fig. S3 in the supplemental material).

As an alternative strategy to address a possible link among DDX1, transcription, and DNA DSBs, we tested the effect of actinomycin D on the formation of DDX1 IRIF. Actinomycin D targets transcription templates by preferentially intercalating into d(GpC) at "transcription bubbles," thus blocking transcription. At 6 $\mu\text{g/ml}$, actinomycin D inhibits transcription by RNA polymerases I, II, and III. HeLa cells were treated with 6 $\mu\text{g/ml}$ of actinomycin D for 30 min prior to exposure to 5 Gy of IR. Cells were then immunostained with anti-DDX1 and anti- $\gamma\text{-H2AX}$ antibodies. Whereas $\gamma\text{-H2AX}$ foci were abundant in actinomycin D-treated irradiated cells, anti-DDX1 immunostaining revealed a speckled pattern without discrete foci (Fig. 5A). The absence of DDX1 IRIF suggests a dependence on RNA transcription.

We also tested whether DDX1 IRIF could form during mitosis, a stage of the cell cycle when there is no RNA synthesis (29, 53). Ten hours after being released from a thymidine block (with $\sim 60\%$ of cells in mitosis), cells were irradiated and immunostained. As shown in Fig. 5B, DDX1 IRIF were not detected in mitotic cells, although IR-induced $\gamma\text{-H2AX}$ IRIF were readily apparent in these cells. Note that the numbers and appearance of DDX1 IRIF are completely normal in the two interphase cells flanking the mitotic cell in Fig. 5B.

RNase H treatment dissociates DDX1 from the IRIF. To further investigate a possible role for RNA in the formation of DDX1 foci in response to IR, we tested the effects of DNase I and RNases A and H on the formation of DDX1 IRIF. HeLa cells exposed to 5 Gy of IR were permeabilized with 2% Tween

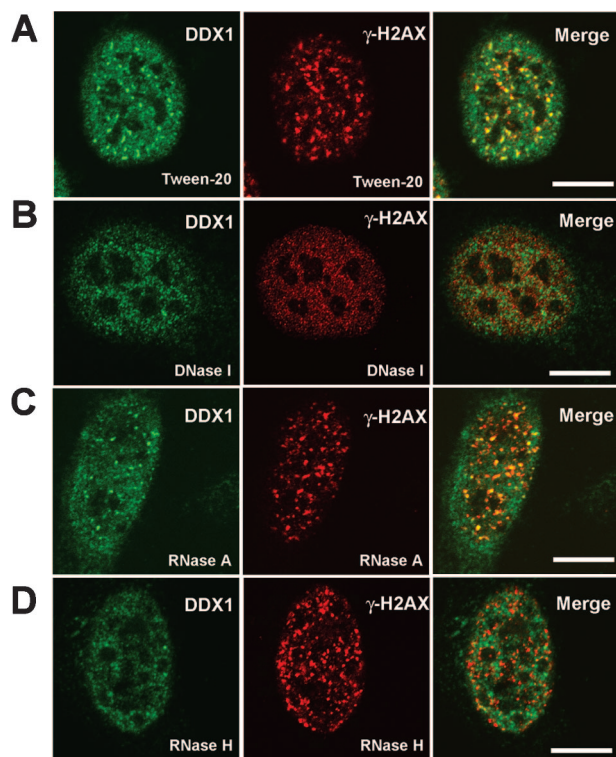


FIG. 6. RNase H treatment dissociates DDX1 from IRIF. HeLa cells were treated with IR (5 Gy) and incubated at 37°C for 1 h to allow the IRIF to form. Cells were then permeabilized (using 2% Tween 20) (A) and treated with DNase I (B), RNase A (C), or RNase H (D). Cells were fixed and immunostained with anti-DDX1 and anti- $\gamma\text{-H2AX}$ antibodies. Bars, 10 μm .

20 and incubated with DNase I, RNase A, or RNase H for 15 min (Fig. 6). The cells were then fixed and immunostained with anti- $\gamma\text{-H2AX}$ and anti-DDX1 antibodies. Consistent with the data in a previous report (61), DNase I digestion abolished IR-induced $\gamma\text{-H2AX}$ foci. DNase I-treated cells were also completely devoid of DDX1 IRIF (Fig. 6B), indicating that both $\gamma\text{-H2AX}$ and DDX1 IRIF depend on the presence of chromosomal DNA for their proper localization. RNase A, which digests single-stranded RNAs, had no effect on IR-induced $\gamma\text{-H2AX}$ and DDX1 foci (Fig. 6C). However, RNase H treatment resulted in the dissociation of DDX1 IRIF, but not $\gamma\text{-H2AX}$ foci, in $\sim 80\%$ cells (Fig. 6D). As RNase H specifically degrades RNA molecules in RNA-DNA duplexes, the dissociation of DDX1 from the IRIF upon RNase H digestion suggests that RNA-DNA duplex structure is required for the maintenance of DDX1 at the DNA DSB sites.

DDX1 unwinds RNA-DNA and RNA-RNA duplexes in vitro. The results from the RNase H treatment suggest that DDX1 at IRIF is involved in binding, unwinding, or otherwise altering RNA-DNA duplex structures. To investigate a possible role for DDX1 in RNA-DNA unwinding, we carried out in vitro unwinding assays using an RNA-DNA hybrid consisting of a 41-nucleotide (nt) RNA strand and a 29-nt DNA strand, with 29 bp of double-stranded structure and a 12-nt RNA overhang at the 5' end (Table 1). R41(+)/D29(-)* (where * denotes the ^{32}P -labeled strand) was purified from an acrylamide gel and

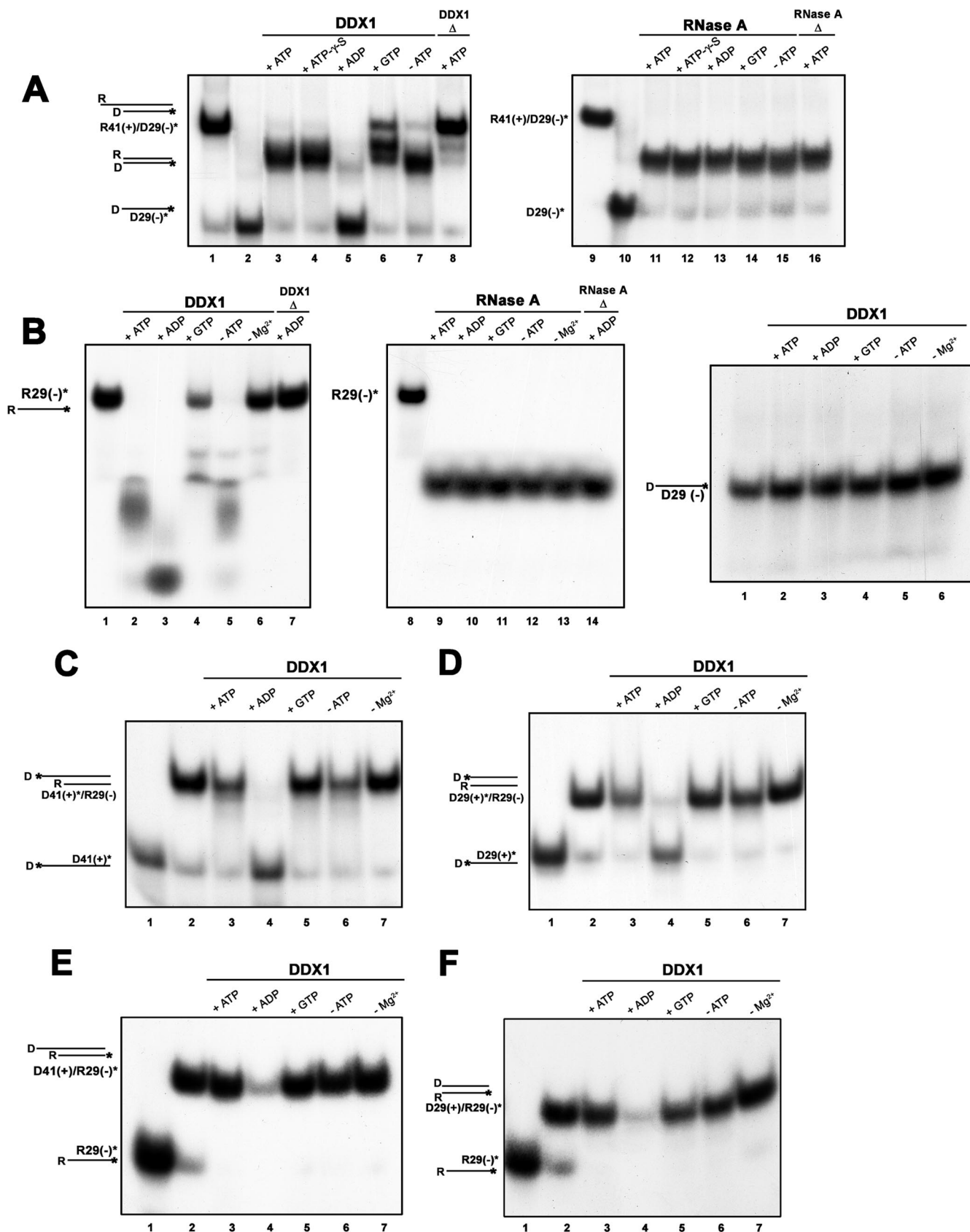


FIG. 7. Characterization of DDX1 RNA-DNA-unwinding activity. (A) The RNA-DNA duplex R41(+)/D29(-)* was generated by the annealing of R41(+) with 5'-end ³²P-labeled D29(-) as described in Materials and Methods. Fifty femtomoles of duplexes was incubated with

incubated with recombinant DDX1. While addition of DDX1 resulted in a band that migrated faster than the RNA-DNA hybrid alone (Fig. 7A, compare lanes 1 and 3), this band migrated at a considerably slower rate than the band corresponding to single-stranded D29 (Fig. 7A, compare lanes 2 and 3), suggesting RNase activity rather than unwinding activity. There was no difference in band migration whether ATP was included in the reaction mixture (Fig. 7A, lane 7), indicating that the nuclease activity is ATP independent. DDX1 was inactivated by boiling, resulting in mostly intact R41/D29 products (Fig. 7A, lane 8). Next, we tested the effects of different nucleotides (ATP, GTP, CTP, UTP, ADP, GDP, and AMP, as well as nonhydrolyzable ATP- γ -S) on DDX1 activity. Data obtained with CTP, GDP, AMP, and ATP- γ -S were similar to those obtained in the presence of ATP or the complete absence of nucleotides (Fig. 7A, lane 4, and data not shown). Both GTP and UTP had an inhibitory effect on DDX1 nuclease activity, with GTP being the stronger inhibitor (Fig. 7A, lane 6, and data not shown). However, the most striking effect was that of ADP, with virtually complete unwinding of the R41/D29 duplex observed in the presence of this nucleotide (Fig. 7A, lane 5). To ensure that these enzymatic activities were not caused by RNase contamination of our DDX1 preparations, we tested the effect of RNase A on the R41/D29 substrate. As shown in Fig. 7A (lanes 9 to 16), a single product migrating approximately halfway between the R41/D29 and D29 bands was observed under all conditions tested. As RNase A cleaves single-stranded RNAs at C and U residues, this product likely represents the R29/D29 heteroduplex.

The banding patterns observed upon the incubation of DDX1 with R41/D29 suggest two activities: an ATP-independent, GTP-inhibited nuclease activity responsible for removing the 5' single-stranded RNA overhang and an ADP-dependent RNA-DNA-unwinding activity. To further address DDX1 nuclease activity, we incubated DDX1 with single-stranded R29(-)* under different buffer conditions. As shown in Fig. 7B, DDX1 effectively digested this substrate in an ATP-independent manner (lanes 2 and 5). R29 degradation was inhibited by GTP (Fig. 7B, lane 4), strictly dependent on Mg²⁺ (Fig. 7B, lane 6), and abolished when DDX1 was boiled for 2 min (Fig. 7B, lane 7). Incubation with ADP resulted in the formation of smaller digestion products than those observed with ATP (Fig. 7B, lane 3). In comparison, the incubation of R29(-)* with RNase A resulted in the complete disappearance of R29, with the same rapidly migrating band observed under all conditions tested (Fig. 7B, lanes 8 to 14). The incubation of DDX1 with the DNA counterpart of R29, D29(-)* (Table 1), revealed no DNase activity under any of the conditions tested (Fig. 7B, far-right panel).

To further characterize the RNA-DNA-unwinding activity

of DDX1, we generated two heteroduplexes: (i) D41(+)/R29(-), with the same nucleotide sequences as the R41(+)/D29(-) duplex but with a 12-nt DNA overhang at the 5' end (Fig. 7C and E), and (ii) blunt-ended D29(+)/R29(-) (Fig. 7D and F). When the DNA strands were labeled, we observed effective unwinding of both the D41/R29 (Fig. 7C) and D29/R29 (Fig. 7D) duplexes in the presence of DDX1 and ADP but not under any of the other conditions tested. When the RNA strands were labeled, significant reductions in the levels of both the D41(+)/R29(-)* and D29(+)/R29(-)* duplexes were observed upon incubation with DDX1 in the presence of ADP (Fig. 7E and F, lanes 4). The absence of single-stranded R29(-)* products in lanes 4 in Fig. 7E and F reflects the single-stranded-RNA degradation activity of DDX1 once the double-stranded molecules had been unwound. In contrast to the RNA-DNA duplex with an RNA overhang (Fig. 7A), where the RNA overhang was digested in a nucleotide-independent manner by DDX1, the D41(+)/R29(-)* duplex remained intact under all conditions tested except when incubated in the presence of ADP. These observations are in keeping with the inability of DDX1 to degrade single-stranded DNA. Together, the results obtained with all three RNA-DNA duplexes tested indicate that overhangs are dispensable for DDX1-mediated unwinding.

As DEAD box proteins are classically defined as RNA helicases or RNA-unwinding/destabilizing proteins, we tested the effect of DDX1 on an RNA-RNA duplex. R41(+)/R29(-)* was generated by annealing R41(+) with ³²P-labeled R29(-) (Table 1). The incubation of this substrate with DDX1 produced results similar to those observed with the R41(+)/D29(-)* duplex: i.e., largely ATP-independent degradation of the 5' RNA overhang (Fig. 8A, lanes 3 and 6) and complete unwinding of the 29-bp double-stranded RNA in the presence of ADP, followed by the degradation of the single-stranded products (Fig. 8A, lane 4). In comparison, RNase A digestion of the RNA-RNA duplex generated similarly migrating bands [representing double-stranded R29(+)/R29(-)*] under all conditions tested (Fig. 8A, lanes 9 to 12). In Fig. 8B, we show that DDX1 cannot degrade or unwind a DNA-DNA duplex prepared by hybridizing D41(+) to ³²P-labeled D29(-)* (Table 1). DNA-DNA duplexes with as few as 16 bp of double-stranded structure could not be unwound by DDX1 (data not shown).

DISCUSSION

Recruitment of DDX1 to sites of DNA DSBs. To this day, DEAD box proteins remain a puzzling family of proteins. In spite of having reasonably well characterized biochemical functions (as ATPases and RNA helicases), the great majority of

either 0.3 μ g of recombinant DDX1 protein (lanes 3 to 8) or 0.1 U of RNase A (lanes 11 to 16) in the presence of 1 mM ATP, ATP- γ -S, ADP, or GTP as indicated. The R41(+)/D29(-)* duplex in lanes 1 and 9 and the D29(-)* oligonucleotide in lanes 2 and 10 were incubated in unwinding buffer without protein. Reaction mixtures containing heat-denatured DDX1 (boiled for 2 min) or RNase A (also boiled for 2 min) are indicated by the symbol Δ (lanes 8 and 16). All reaction mixtures were incubated for 20 min at 37°C prior to electrophoresis in a 12% polyacrylamide gel, followed by autoradiography. R, RNA; D, DNA; +, with; -, without. (B) Fifty femtomoles of 5'-end ³²P-labeled R29(-) was incubated with either 0.3 μ g of recombinant DDX1 (lanes 2 to 7) or 0.1 U of RNase A (lanes 9 to 14). Mg²⁺ was omitted in lanes 6 and 13. Heat-denatured DDX1 and RNase A were used in lanes 7 and 14, respectively. (C to F) Reactions were carried out with 0.3 μ g of DDX1 and D41(+)*R29(-) (C), D29(+)*R29(-) (D), D41(+)/R29(-)* (E), and D29(+)/R29(-)* (F), as described in the legend to panel A.

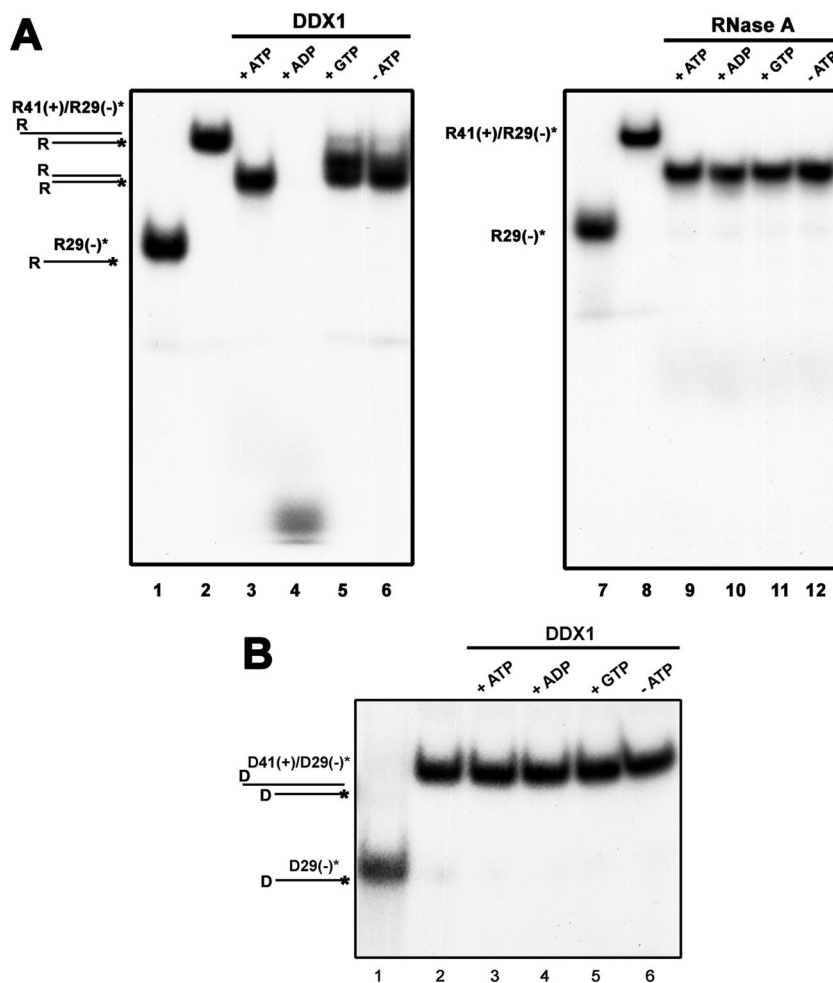


FIG. 8. DDX1 unwinds RNA-RNA but not DNA-DNA duplexes. (A) The RNA-RNA duplex R41(+)/R29(-)* was generated by annealing R41(+) with 5'-end ^{32}P -labeled R29(-). Fifty femtomoles of the substrate was incubated with either 0.3 μg of recombinant DDX1 (lanes 3 to 6) or 0.1 U of RNase A (lanes 9 to 12) in the presence of 1 mM ATP, ADP, or GTP as indicated. The R29(-)* oligonucleotide in lanes 1 and 7 and the R41(+)/R29(-)* duplex in lanes 2 and 8 were incubated in unwinding buffer without protein. ATP was omitted from reaction mixtures loaded into lanes 6 and 12. All reactions were carried out for 20 min at 37°C prior to electrophoresis in a 12% polyacrylamide gel, followed by autoradiography. R, RNA; D, DNA; +, with; -, without. (B) Fifty femtomoles of D41(+)/D29(-)* was incubated with 0.3 μg of recombinant DDX1 (lanes 2 to 6) at 37°C for 20 min, and the mixture was then subjected to electrophoresis and autoradiography.

these proteins have no clear biological roles. Few natural RNA substrates for DEAD box proteins have been identified, perhaps reflecting transient interactions with a wide spectrum of RNAs or simply our lack of understanding of the complex environment under which these proteins operate. Here, we demonstrate that DDX1 is part of the intricate machinery that is rapidly engaged when a cell is exposed to agents that cause DNA DSBs. Similar to pATM and $\gamma\text{-H2AX}$, DDX1 is recruited to sites of DNA DSBs within minutes of the cell's being exposed to IR, suggesting a requirement for DDX1 early in the DNA damage response. DDX1 IRIF are also observed when cells are exposed to the radiomimetic drug bleomycin. In contrast, exposure to UV and cisplatin does not initially lead to DDX1 IRIF formation, although DDX1 IRIF form at later time points, presumably at sites of unrepaired DNA damage resulting in DSBs. These combined data suggest a role for DDX1 that is specific to DNA DSBs.

Role of ATM in DDX1 recruitment to sites of DNA DSBs.

The cellular response to DNA DSBs involves a well-orchestrated series of signaling events, from checkpoint activation and cell cycle arrest to the repair of the damaged DNA and the resumption of cell cycle progression. ATM is a key player in damage sensing, signal transduction, and the coordination of the diverse pathways that are part of the DSB response (33, 54). The main mechanism by which ATM relays damage signals is the direct phosphorylation of its substrate proteins. The complete absence of DDX1 IRIF in ATM-defective cells, combined with the fact that at least some DDX1 exists in a complex with ATM, suggests that DDX1 may be a substrate of ATM. In support of this possibility, we have shown that DDX1 is phosphorylated by endogenous ATM *in vitro* and that DDX1 phosphorylation is dependent on Mn^{2+} and inhibited by wortmannin, both characteristics of ATM kinase phosphorylation (5). Furthermore, DDX1 phosphorylation is induced *in vivo* upon

the exposure of cells to IR, and this response is inhibited by wortmannin. These data are compatible with the direct mediation of the recruitment of DDX1 to DSBs through ATM phosphorylation. However, we cannot exclude the possibility that the recruitment of DDX1 to these sites is an indirect consequence of the ATM-mediated phosphorylation of other proteins. Two recent studies involving systematic searches for ATM substrates in DNA DSB-induced cellular responses have yielded hundreds of putative novel ATM interactors (39, 40). It is noteworthy that a number of DEAD box proteins (DDX6, DDX17, DDX18, and DDX47) were identified in these screens, suggesting a broad-scope relationship between DEAD box proteins and ATM.

DNA/RNA helicases in the DNA damage response. DNA helicases implicated in the DNA damage response include RecQ DNA helicases BLM, WRN, and RECQL4, as well as a DEAxQ helicase called senataxin (57). BLM, defective in individuals with Bloom's syndrome, interacts directly with ATM and exhibits ATM-dependent phosphorylation upon IR (9). At sites of DNA breaks, BLM disrupts the Rad51–single-stranded-DNA filament, a species that promotes HR (13). As BLM can also stimulate DNA repair, it has been suggested previously that BLM plays a dual function in promoting and inhibiting HR (13).

A few reports indicate a possible role for DEAD box proteins in the DNA DSB response. For example, Ghabrial and Schupbach (23) suggested that Vasa (DDX4) in *Drosophila melanogaster* may be a target of a meiotic checkpoint that is activated by the accumulation of DNA DSBs. In addition, the results of studies using human p68 (DDX5) indicate that this DEAD box protein may be required for p53-regulated gene expression upon exposure to etoposide, a DNA DSB-inducing agent (8). The data presented here provide evidence that DDX1 plays an integral role in the cellular response to DNA DSBs. However, only a subset of DNA DSBs are targeted by DDX1, as evidenced by the fact that only 29% of γ -H2AX IRIF colocalized with DDX1 IRIF. Strikingly, RNase H and DNase I treatment, but not RNase A treatment, eliminated DDX1 IRIF. As RNase H removes RNA from RNA-DNA double-stranded molecules, these results suggest a requirement for both DNA and RNA at sites of DDX1 IRIF. The involvement of RNA at DNA DSBs has been reported previously by Pryde et al. (44), who demonstrated that treatment with RNase A, but not RNase H, dissociates 53BP1 from IRIF. These authors proposed that RNA is required for 53BP1 retention at DSBs. The results obtained with 53BP1 and DDX1 suggest different types of nucleic acid interactions among the proteins recruited at DNA DSBs.

Recruitment of DDX1 to sites of DNA DSBs containing RNA. There are an estimated 5,000 to 8,000 actively transcribed genes in the nucleus of a cycling HeLa cell (17). These genes are believed to be transcribed in foci enriched with RNA polymerase II, called transcription factories (28). Although the effect of DSBs on transcription remains poorly understood, one would expect either stalling or dismantling of the transcriptional machinery in the general vicinity of DNA DSBs. A coimmunostaining analysis did not reveal any colocalization of RNA polymerase II and DDX1, either before or after irradiation. Furthermore, our 5-FUrd incorporation analysis indicates that there is no enrichment of newly synthesized RNA at

DDX1 IRIF. As the limit of detection of the confocal microscopy is $\sim 0.2 \mu\text{m}$, thus requiring thousands of fluorescently labeled molecules for detection, the only conclusion one can reach from these studies is that there is no accumulation of large quantities of newly synthesized RNA at DDX1 IRIF.

In keeping with a need for RNA at DDX1 IRIF, actinomycin D, a drug that intercalates into double-stranded DNA at the transcription bubble and interferes with RNA elongation by all three RNA polymerases, effectively inhibited DDX1 (but not γ -H2AX) IRIF formation. Others have shown that RNA is released from its site of transcription within minutes of being exposed to actinomycin D (19). Interestingly, actinomycin D itself can induce the formation of γ -H2AX foci and has been proposed to distort DNA structures at transcriptionally active sites (42). Of note, cells in mitosis, the only stage of the cell cycle when transcription is silent, did not undergo DDX1 IRIF formation. Together with the RNase H results discussed earlier, our data support a role for RNA in the recruitment or retention of DDX1 at DNA DSBs.

DDX1 can unwind RNA-DNA substrates. In a previous study, recombinant DDX1 was unable to unwind RNA-RNA duplexes containing either 10 or 14 bp of complementary sequence (16). Here we have shown that DDX1 can unwind both RNA-RNA and RNA-DNA duplexes containing 29 bp of double-stranded structure in an ADP-dependent manner. Furthermore, in addition to unwinding activity, DDX1 has an ATP/ADP-independent RNase activity toward single-stranded RNA that is inhibited by GTP and requires Mg^{2+} . Although no other DEAD box proteins with unwinding and RNase activities have been described in the literature to date, the WRN DNA helicase has been reported to have a 5'→3' exonuclease activity that removes one DNA strand in a DNA-DNA duplex and the RNA strand in an RNA-DNA duplex (58). In contrast to DDX1, WRN does not digest single-stranded RNA (or DNA), and its exonuclease activity is dependent on unwinding.

Other DEAD box proteins have been shown to have both RNA-RNA- and RNA-DNA-unwinding activities. For example, eIF4A can unwind both RNA-RNA and RNA-DNA duplexes containing 12 to 17 bp of double-stranded structure in the presence of ATP (49). Yeast Has1p, a DEAD box protein involved in 18S rRNA maturation, unwinds RNA-DNA duplexes containing 16 to 17 bp of double-stranded structure, also in an ATP-dependent manner (46). While most DEAD box proteins unwind RNA-RNA or RNA-DNA duplexes in an ATP-dependent manner, a requirement for ADP is not without precedent. For example, the RNA-unwinding and -annealing activities of yeast DEAD box protein DED1 have recently been shown to be controlled by relative ATP and ADP concentrations (62). Although ADP itself does not allow DED1 to unwind RNA, a higher ADP concentration promotes annealing over unwinding. A second yeast DEAD box protein, Dbp5, appears to function in a manner analogous to that of Ran, shifting between ATP-bound and ADP-bound states (59). The ADP-bound form of Dbp5 is required for RNP remodeling, with ADP-bound Dbp5 having a different conformation from that of ATP-bound Dbp5.

Role of DDX1 at DNA DSBs. The two main pathways involved in DNA DSB repair are error-prone nonhomologous end joining and HR, which involves template-guided repair using undamaged homologous sequences. Although few stud-

ies have addressed heterogeneity in the repair of DNA DSBs, one could surmise that it would be of benefit to the cell to use a template-guided mechanism for the repair of transcriptionally active genes. In fact, it has been suggested previously that only DSBs associated with transcription can induce the chromosomal exchange events related to HR (45). Template-guided repair requires the unwinding of the DNA double strands to allow the copying of the undamaged DNA into the damaged DNA strand. Unwound DNA may be particularly susceptible to binding with complementary transcripts. Conversely, RNA released from transcription factories as the result of DNA DSBs may be particularly prone to pairing with its complementary genomic DNA. DDX1 may therefore play a role in clearing DNA of opportunistic DNA-RNA interactions resulting from DSBs. In this context, DDX1 may play an active role in template-guided repair or may simply facilitate the replacement of the transcription machinery with the DNA repair machinery.

DDX1 accumulated at a subset of DNA DSBs which invariably (that is, in the case of >90% of DDX1 IRIF) contained pATM. As DDX1 IRIF did not form in the absence of ATM, we propose the following model. DDX1 is phosphorylated and recruited to DNA DSBs by ATM. The presence of DNA-RNA duplex structures at DSB sites is critical for the retention of DDX1. Relative enrichment with and/or the accessibility of ADP at these sites activates DDX1 unwinding activity, likely through a conformational alteration of DDX1 as observed previously for other ADP binding proteins (4, 59). The RNA-DNA-unwinding activity of DDX1, combined with its RNase activity, ensures the complete removal and degradation of RNA from these sites. Thus, we propose a role for DDX1 in RNA clearance from sites of DSBs to facilitate repair. In support of this model, a role in RNA clearance has recently been proposed for *Drosophila* DEAD box protein DDX5 (p68), specifically to remove RNA from transcribed genes in order to reset the chromatin to a transcriptionally inactive state (14).

In summary, we have shown that DDX1 rapidly accumulates at sites of DNA DSBs in an ATM-dependent manner upon exposure to IR. DDX1 has ADP-dependent RNA-DNA- and RNA-RNA-unwinding activities, as well as ADP/ATP-independent RNase activity toward single-stranded RNA. Our data suggest that the presence of RNA at DNA DSBs is a prerequisite for DDX1 recruitment at these sites. We propose that the combined RNase and RNA-DNA-unwinding activities of DDX1 provide a powerful tool for the rapid clearance of RNA from sites of DNA DSBs, thus facilitating DSB repair. Determining whether DDX1 marks RNA-containing DNA DSB sites for special repair, e.g., by a template-guided mechanism, will be the subject of future investigations.

ACKNOWLEDGMENTS

We thank Joan Turner and Rufus Day for the M059J and M059K malignant glioma cell lines, Susan Lees-Miller for the BT and L3 lymphoblastoid cell lines, Yosef Shiloh for the EBS and YZ5 cell lines, Razmik Mirzayans for the AT2BE and AT5BI fibroblast cultures from A-T patients, Charlotte Spencer for the anti-RNA polymerase II antibody, James L. Manley for the anti-CstF64 antibody, Roel van Driel for the anti-PML antibody, Joan Steitz for the anti-Sm Y12 antibody, Joan Turner and Jianxun Han for the anti-ATM antibody used for the immunoprecipitation experiments, and Charles Holmes for the microcystin-LR. We are grateful to Kenneth Roy for expert technical assistance. We are indebted to Sachin Katyal, Joan Turner, Michael Hendzed, and Linda Reha-Krantz for helpful comments.

This work was supported by a grant from the Alberta Cancer Research Institute. L.L. is the recipient of an Alberta Cancer Research Institute fellowship.

REFERENCES

- Abdelhaleem, M., L. Maltais, and H. Wain. 2003. The human DDX and DHX gene families of putative RNA helicases. *Genomics* **81**:618–622.
- Abraham, R. T. 2004. PI 3-kinase related kinases: 'big' players in stress-induced signaling pathways. *DNA Repair (Amsterdam)* **3**:883–887.
- Bakkenist, C. J., and M. B. Kastan. 2003. DNA damage activates ATM through intermolecular autophosphorylation and dimer dissociation. *Nature* **421**:499–506.
- Banerjee, S., T. Schmidt, J. Fang, C. A. Stanley, and T. J. Smith. 2003. Structural studies on ADP activation of mammalian glutamate dehydrogenase and the evolution of regulation. *Biochemistry* **42**:3446–3456.
- Banin, S., L. Moyal, S. Shieh, Y. Taya, C. W. Anderson, L. Chessa, N. I. Smorodinsky, C. Prives, Y. Reiss, Y. Shiloh, and Y. Ziv. 1998. Enhanced phosphorylation of p53 by ATM in response to DNA damage. *Science* **281**:1674–1677.
- Barfknecht, T. R., and J. B. Little. 1982. Hypersensitivity of ataxia telangiectasia skin fibroblasts to DNA alkylating agents. *Mutat. Res.* **94**:369–382.
- Bartek, J., C. Lukas, and J. Lukas. 2004. Checking on DNA damage in S phase. *Nat. Rev. Mol. Cell Biol.* **5**:792–804.
- Bates, G. J., S. M. Nicol, B. J. Wilson, A. M. Jacobs, J. C. Bourdon, J. Wardrop, D. J. Gregory, D. P. Lane, N. D. Perkins, and F. V. Fuller-Pace. 2005. The DEAD box protein p68: a novel transcriptional coactivator of the p53 tumour suppressor. *EMBO J.* **24**:543–553.
- Beamish, H., P. Kedar, H. Kaneko, P. Chen, T. Fukao, C. Peng, S. Beresten, N. Gueven, D. Purdie, S. Lees-Miller, N. Ellis, N. Kondo, and M. F. Lavin. 2002. Functional link between BLM defective in Bloom's syndrome and the ataxia-telangiectasia-mutated protein, ATM. *J. Biol. Chem.* **277**:30515–30523.
- Bergkessel, M., and J. C. Reese. 2004. An essential role for the *Saccharomyces cerevisiae* DEAD-box helicase DHH1 in G1/S DNA-damage checkpoint recovery. *Genetics* **167**:21–33.
- Bleoo, S., X. Sun, M. J. Hendzel, J. M. Rowe, M. Packer, and R. Godbout. 2001. Association of human DEAD box protein DDX1 with a cleavage stimulation factor involved in 3'-end processing of pre-mRNA. *Mol. Biol. Cell* **12**:3046–3059.
- Bregman, D. B., L. Du, S. van der Zee, and S. L. Warren. 1995. Transcription-dependent redistribution of the large subunit of RNA polymerase II to discrete nuclear domains. *J. Cell Biol.* **129**:287–298.
- Bugreev, D. V., X. Yu, E. H. Egelman, and A. V. Mazin. 2007. Novel pro- and anti-recombination activities of the Bloom's syndrome helicase. *Genes Dev.* **21**:3085–3094.
- Buszczak, M., and A. C. Spradling. 2006. The *Drosophila* P68 RNA helicase regulates transcriptional deactivation by promoting RNA release from chromatin. *Genes Dev.* **20**:977–989.
- Canman, C. E., D. S. Lim, K. A. Cimprich, Y. Taya, K. Tamai, K. Sakaguchi, E. Appella, M. B. Kastan, and J. D. Siliciano. 1998. Activation of the ATM kinase by ionizing radiation and phosphorylation of p53. *Science* **281**:1677–1679.
- Chen, H. C., W. C. Lin, Y. G. Tsay, S. C. Lee, and C. J. Chang. 2002. An RNA helicase, DDX1, interacting with poly(A) RNA and heterogeneous nuclear ribonucleoprotein K. *J. Biol. Chem.* **277**:40403–40409.
- Cook, P. R. 1999. The organization of replication and transcription. *Science* **284**:1790–1795.
- Cortez, D., Y. Wang, J. Qin, and S. J. Elledge. 1999. Requirement of ATM-dependent phosphorylation of brca1 in the DNA damage response to double-strand breaks. *Science* **286**:1162–1166.
- Custodio, N., M. Carmo-Fonseca, F. Geraghty, H. S. Pereira, F. Grosveld, and M. Antoniou. 1999. Inefficient processing impairs release of RNA from the site of transcription. *EMBO J.* **18**:2855–2866.
- Dellaire, G., R. W. Ching, K. Ahmed, F. Jalali, K. C. Tse, R. G. Bristow, and D. P. Bazett-Jones. 2006. Promyelocytic leukemia nuclear bodies behave as DNA damage sensors whose response to DNA double-strand breaks is regulated by NBS1 and the kinases ATM, Chk2, and ATR. *J. Cell Biol.* **175**:55–66.
- Falck, J., J. Coates, and S. P. Jackson. 2005. Conserved modes of recruitment of ATM, ATR and DNA-PKcs to sites of DNA damage. *Nature* **434**:605–611.
- Gall, J. G. 2000. Cajal bodies: the first 100 years. *Annu. Rev. Cell Dev. Biol.* **16**:273–300.
- Ghabrial, A., and T. Schupbach. 1999. Activation of a meiotic checkpoint regulates translation of Gurken during *Drosophila* oogenesis. *Nat. Cell Biol.* **1**:354–357.
- Gingras, A. C., B. Raught, and N. Sonenberg. 1999. eIF4 initiation factors: effectors of mRNA recruitment to ribosomes and regulators of translation. *Annu. Rev. Biochem.* **68**:913–963.
- Godbout, R., L. Li, R. Z. Liu, and K. Roy. 2007. Role of DEAD box 1 in retinoblastoma and neuroblastoma. *Future Oncol.* **3**:575–587.

26. **Godbout, R., and J. Squire.** 1993. Amplification of a DEAD box protein gene in retinoblastoma cell lines. *Proc. Natl. Acad. Sci. USA* **90**:7578–7582.
27. **Hurley, P. J., and F. Bunz.** 2007. ATM and ATR: components of an integrated circuit. *Cell Cycle* **6**:414–417.
28. **Jackson, D. A., A. B. Hassan, R. J. Errington, and P. R. Cook.** 1993. Visualization of focal sites of transcription within human nuclei. *EMBO J.* **12**:1059–1065.
29. **Johnson, T. C., and J. J. Holland.** 1965. Ribonucleic acid and protein synthesis in mitotic HeLa cells. *J. Cell Biol.* **27**:565–574.
30. **Khanna, K. K., and S. P. Jackson.** 2001. DNA double-strand breaks: signaling, repair and the cancer connection. *Nat. Genet.* **27**:247–254.
31. **Kim, S. T., D. S. Lim, C. E. Canman, and M. B. Kastan.** 1999. Substrate specificities and identification of putative substrates of ATM kinase family members. *J. Biol. Chem.* **274**:37538–37543.
32. **Kozlov, S. V., M. E. Graham, C. Peng, P. Chen, P. J. Robinson, and M. F. Lavin.** 2006. Involvement of novel autophosphorylation sites in ATM activation. *EMBO J.* **25**:3504–3514.
33. **Kurz, E. U., and S. P. Lees-Miller.** 2004. DNA damage-induced activation of ATM and ATM-dependent signaling pathways. *DNA Repair (Amsterdam)* **3**:889–900.
34. **Lavin, M. F., and Y. Shiloh.** 1997. The genetic defect in ataxia-telangiectasia. *Annu. Rev. Immunol.* **15**:177–202.
35. **Lee, J. H., and T. T. Paull.** 2005. ATM activation by DNA double-strand breaks through the Mre11-Rad50-Nbs1 complex. *Science* **308**:551–554.
36. **Lees-Miller, S. P., R. Godbout, D. W. Chan, M. Weinfeld, R. S. Day III, G. M. Barron, and J. Allalunis-Turner.** 1995. Absence of p350 subunit of DNA-activated protein kinase from a radiosensitive human cell line. *Science* **267**:1183–1185.
37. **Li, L., K. Roy, S. Katyal, X. Sun, S. Bleoo, and R. Godbout.** 2006. Dynamic nature of cleavage bodies and their spatial relationship to DDX1 bodies, Cajal bodies, and gems. *Mol. Biol. Cell* **17**:1126–1140.
38. **Linder, P.** 2006. Dead-box proteins: a family affair—active and passive players in RNP-remodeling. *Nucleic Acids Res.* **34**:4168–4180.
39. **Linding, R., L. J. Jensen, G. J. Ostheimer, M. A. van Vugt, C. Jorgensen, I. M. Miron, F. Diella, K. Colwill, L. Taylor, K. Elder, P. Metalnikov, V. Nguyen, A. Pasculescu, J. Jin, J. G. Park, L. D. Samson, J. R. Woodgett, R. B. Russell, P. Bork, M. B. Yaffe, and T. Pawson.** 2007. Systematic discovery of in vivo phosphorylation networks. *Cell* **129**:1415–1426.
40. **Matsuoka, S., B. A. Ballif, A. Smogorzewska, E. R. McDonald III, K. E. Hurov, J. Luo, C. E. Bakalarski, Z. Zhao, N. Solimini, Y. Lerenthal, Y. Shiloh, S. P. Gygi, and S. J. Elledge.** 2007. ATM and ATR substrate analysis reveals extensive protein networks responsive to DNA damage. *Science* **316**:1160–1166.
41. **Methot, N., A. Pause, J. W. Hershey, and N. Sonenberg.** 1994. The translation initiation factor eIF-4B contains an RNA-binding region that is distinct and independent from its ribonucleoprotein consensus sequence. *Mol. Cell Biol.* **14**:2307–2316.
42. **Mischo, H. E., P. Hemmerich, F. Grosse, and S. Zhang.** 2005. Actinomycin D induces histone gamma-H2AX foci and complex formation of gamma-H2AX with Ku70 and nuclear DNA helicase II. *J. Biol. Chem.* **280**:9586–9594.
43. **Ponting, C., J. Schultz, and P. Bork.** 1997. SPRY domains in ryanodine receptors (Ca²⁺-release channels). *Trends Biochem. Sci.* **22**:193–194.
44. **Pryde, F., S. Khalili, K. Robertson, J. Selfridge, A. M. Ritchie, D. W. Melton, D. Jullien, and Y. Adachi.** 2005. 53BP1 exchanges slowly at the sites of DNA damage and appears to require RNA for its association with chromatin. *J. Cell Sci.* **118**:2043–2055.
45. **Radford, I. R.** 2002. Transcription-based model for the induction of inter-chromosomal exchange events by ionizing irradiation in mammalian cell lines that undergo necrosis. *Int. J. Radiat. Biol.* **78**:1081–1093.
46. **Rocak, S., B. Emery, N. K. Tanner, and P. Linder.** 2005. Characterization of the ATPase and unwinding activities of the yeast DEAD-box protein Has1p and the analysis of the roles of the conserved motifs. *Nucleic Acids Res.* **33**:999–1009.
47. **Rocak, S., and P. Linder.** 2004. DEAD-box proteins: the driving forces behind RNA metabolism. *Nat. Rev. Mol. Cell Biol.* **5**:232–241.
48. **Rogakou, E. P., C. Boon, C. Redon, and W. M. Bonner.** 1999. Megabase chromatin domains involved in DNA double-strand breaks in vivo. *J. Cell Biol.* **146**:905–916.
49. **Rogers, G. W., Jr., W. F. Lima, and W. C. Merrick.** 2001. Further characterization of the helicase activity of eIF4A. Substrate specificity. *J. Biol. Chem.* **276**:12598–12608.
50. **Ruiz de Almodovar, J. M., G. G. Steel, S. J. Whitaker, and T. J. McMillan.** 1994. A comparison of methods for calculating DNA double-strand break induction frequency in mammalian cells by pulsed-field gel electrophoresis. *Int. J. Radiat. Biol.* **65**:641–649.
51. **Sarkaria, J. N., R. S. Tibbetts, E. C. Busby, A. P. Kennedy, D. E. Hill, and R. T. Abraham.** 1998. Inhibition of phosphoinositide 3-kinase related kinases by the radiosensitizing agent wortmannin. *Cancer Res.* **58**:4375–4382.
52. **Schurer, K. A., C. Rudolph, H. D. Ulrich, and W. Kramer.** 2004. Yeast MPH1 gene functions in an error-free DNA damage bypass pathway that requires genes from homologous recombination, but not from postreplicative repair. *Genetics* **166**:1673–1686.
53. **Shermoen, A. W., and P. H. O'Farrell.** 1991. Progression of the cell cycle through mitosis leads to abortion of nascent transcripts. *Cell* **67**:303–310.
54. **Shiloh, Y.** 2006. The ATM-mediated DNA-damage response: taking shape. *Trends Biochem. Sci.* **31**:402–410.
55. **Simons, J. W.** 1979. Development of a liquid-holding technique for the study of DNA-repair in human diploid fibroblasts. *Mutat. Res.* **59**:273–283.
56. **Stiff, T., M. O'Driscoll, N. Rief, K. Iwabuchi, M. Lobrich, and P. A. Jeggo.** 2004. ATM and DNA-PK function redundantly to phosphorylate H2AX after exposure to ionizing radiation. *Cancer Res.* **64**:2390–2396.
57. **Suraweera, A., O. J. Becherel, P. Chen, N. Rundle, R. Woods, J. Nakamura, M. Gatei, C. Criscuolo, A. Filla, L. Chessa, M. Fusser, B. Epe, N. Gueven, and M. F. Lavin.** 2007. Senataxin, defective in ataxia oculomotor apraxia type 2, is involved in the defense against oxidative DNA damage. *J. Cell Biol.* **177**:969–979.
58. **Suzuki, N., M. Shiratori, M. Goto, and Y. Furuichi.** 1999. Werner syndrome helicase contains a 5'→3' exonuclease activity that digests DNA and RNA strands in DNA/DNA and RNA/DNA duplexes dependent on unwinding. *Nucleic Acids Res.* **27**:2361–2368.
59. **Tran, E. J., Y. Zhou, A. H. Corbett, and S. R. Wente.** 2007. The DEAD-box protein Dbp5 controls mRNA export by triggering specific RNA:protein remodeling events. *Mol. Cell* **28**:850–859.
60. **Ward, I. M., and J. Chen.** 2001. Histone H2AX is phosphorylated in an ATR-dependent manner in response to replicational stress. *J. Biol. Chem.* **276**:47759–47762.
61. **Ward, I. M., K. Minn, K. G. Jorda, and J. Chen.** 2003. Accumulation of checkpoint protein 53BP1 at DNA breaks involves its binding to phosphorylated histone H2AX. *J. Biol. Chem.* **278**:19579–19582.
62. **Yang, Q., and E. Jankowsky.** 2005. ATP- and ADP-dependent modulation of RNA unwinding and strand annealing activities by the DEAD-box protein DED1. *Biochemistry* **44**:13591–13601.
63. **Ziv, Y., A. Bar-Shira, I. Pecker, P. Russell, T. J. Jorgensen, I. Tsarfati, and Y. Shiloh.** 1997. Recombinant ATM protein complements the cellular A-T phenotype. *Oncogene* **15**:159–167.